

PORE-SCALE MODELING OF THREE-PHASE FLOW: COMPARATIVE STUDY WITH EXPERIMENTAL RESERVOIR DATA

C. Nardi⁽¹⁾, O. Lopez⁽¹⁾, P.E. Øren⁽¹⁾, R. Held⁽²⁾ and E. B. Petersen Jr⁽²⁾
⁽¹⁾ Numerical Rocks AS and ⁽²⁾ StatoilHydro ASA

This paper was prepared for presentation at the International Symposium of the Society of Core Analysts held in Noordwijk, The Netherlands 27-30 September, 2009

ABSTRACT

We present a general network model to simulate three-phase capillary dominated processes on pore networks extracted from a digitized representation of the rock microstructure. Important features, such as wettability alteration, hysteresis, intermediate phase spreading layers, and true three-phase capillary entry pressures, are implemented in the model. The model has been used to compute two- and three-phase relative permeabilities of a reconstructed reservoir rock. First, the model is anchored to the experimental two-phase data to yield end point saturations and the pore-scale wettability (i.e. contact angle) distribution. Next, predictions of three-phase relative permeabilities for different displacement processes are made. The computed results are compared with recently acquired experimental data. These data represent two- and three-phase steady-state flow measurements under in-situ conditions on composite core material from the Statfjord field (SCA2008-23) [15].

INTRODUCTION

Three-phase flow in porous media is of sustained theoretical and practical interest in many industrial applications. In oil reservoirs, three-phase flow occurs during gas cap expansion, solution gas drive, gas injection, water alternating gas injection, depressurization below the bubble point, or CO₂ storage. To understand and being able to predict three-phase flow behavior, accurate estimates of constitutive relations such as relative permeability and capillary pressure are needed. In the case of two-phase flow, constitutive relations are routinely measured in the laboratory. Three-phase relations are both difficult and time consuming to determine experimentally, especially under reservoir conditions. Furthermore, it is impractical to measure these relations for the full range of saturations paths that may occur during three-phase flow in the reservoir. As a result, three-phase relative permeabilities are almost always estimated from two-phase data on the basis of empirical models.

Pore-scale modeling offers an alternative to empirical models. Pore-scale or network models can be used to predict multiphase flow behavior by simulating the flow process based on a detailed description of the pore structure, fluid characteristics, and the governing pore-scale displacement mechanisms. For two-phase flow, the predictive capabilities of using rock microstructure images combined with network modelling have been demonstrated on a number of different sandstones. In recent years, three-phase network models [1,2] have been developed and shown to predict with reasonable accuracy the three-phase relative permeability measurements conducted by Oak on water wet Berea outcrop sandstone [3].

In the present work, we describe our preliminary results on the ongoing development of a general network model for simulating three-phase flow directly on pore networks extracted from digitized images of the rock microstructure. The three-phase network model has been implemented to perform any immiscible fluid injection (gas, water or oil), where the initial fluid distribution is established via a two-phase oil-water displacement or by a three-phase displacement process. The model performance is demonstrated by comparing predicted and measured two- and three-phase relative permeabilities of a non-water wet reservoir rock from the Statfjord field.

THREE-PHASE FLOW NETWORK MODEL

The three-phase network model reproduces both drainage and imbibition dominated three-phase flow processes. The three fluids are assumed to be immiscible and incompressible. Furthermore, we assume that capillary forces dominate at the pore-scale, which is a reasonable assumption for capillary numbers in the range of 10^{-6} and below. Finally, we assume that there is no momentum transfer across fluid-fluid interfaces, i.e., we neglect the effects of viscous coupling. In the following, we describe the model functionalities that have been implemented to simulate the three-phase displacement processes. The network model implementation we used to simulate the two-phase displacements has been described previously [4].

Spreading Coefficient and Contact Angles

The ability of oil to spread on water in the presence of gas is governed by the spreading coefficient S_{ow} , defined as

$$S_{ow} = \sigma_{gw} - \sigma_{ow} - \sigma_{go} \quad (1)$$

The spreading coefficient represents the force balance at the three-phase contact line. If the initial spreading coefficient is zero or positive, oil spontaneously spreads between the gas and water to completely wet the water surface (positive spreading system). If the spreading coefficient is negative, the three fluids meet to form a three-phase contact line. Further discussion of spreading systems is given in references [5-7].

In a three-phase fluid system, the horizontal force balance for each of the three fluid pairs residing on a solid can be rewritten to yield the Bartell-Osterhoff Equation [8]

$$\sigma_{gw} \cos \theta_{gw} = \sigma_{ow} \cos \theta_{ow} + \sigma_{go} \cos \theta_{go} \quad (2)$$

where θ is the respective two-phase contact angle measured through the denser phase. In the present analysis, we assume that the oil-water contact angle is known. Gas-water and gas-oil contact angles that satisfy the above constraint must then be derived. Van Dijke et al. [9] presented a linear relationship that satisfies Equation (2) to find the equilibrium gas-oil and gas-water contact angles from the oil-water contact angle and the interfacial tensions

$$\cos \theta_{go} = \frac{1}{2\sigma_{go}} [S_{ow} \cos \theta_{ow} + S_{ow} + 2\sigma_{go}] \quad (3)$$

$$\cos \theta_{gw} = \frac{1}{2\sigma_{gw}} [(S_{ow} + 2\sigma_{ow}) \cos \theta_{ow} + S_{ow} + 2\sigma_{go}] \quad (4)$$

The actual values of the contact angles depend on the direction of the displacement. For mixed-wet systems, the advancing contact angle θ_a can be significantly larger than the receding contact angle θ_r . To describe different displacement processes, six contact angles are assigned to each pore body and throat: $\theta_{a,ow}$ (water displacing oil), $\theta_{r,ow}$ (oil displacing water), $\theta_{a,go}$ (oil displacing gas), $\theta_{r,go}$ (gas displacing oil), $\theta_{a,gw}$ (water displacing gas), and $\theta_{r,gw}$ (gas displacing water). In this work, the advancing and receding oil-water contact angles are determined from the available two-phase data. The corresponding gas-water and gas-oil contact angles can then be computed based on Equations (3) and (4).

Corner Fluid Configurations

Pores with non-circular cross-section allow multiple fluids to be simultaneously present in individual pore elements. In two-phase flow, capillary pressure dictates that the non-wetting fluid occupies the bulk of the pore space, with wetting fluid present in corners of the pore element. In three-phase flow, a pore cross-section may be occupied by one, two or all three fluids simultaneously and a number of different fluid configurations might arise. An overview of all conceivable three-phase fluid configurations is given in [1]. If a pore is occupied by only two fluids, the possible configurations are identical to those previously reported in [4].

When three fluids are present in a pore, the distribution of the fluids is governed by wettability, spreading and capillary pressure. Designating the fluids as 1 = non-wetting, 2 = intermediate wetting and 3 = wetting, a necessary criterion for the presence of an intermediate phase between the wetting and the non-wetting phases is given by [1]

$$\frac{r_{23}}{r_{12}} \leq \frac{\cos(\theta_{12} + \beta)}{\cos(\theta_{23} + \beta)} \quad \text{if } \theta_{23} \leq \theta_{12} \quad (5)$$

$$\frac{r_{23}}{r_{12}} \leq \frac{\cos \theta_{12} - \sin \beta}{\cos \theta_{23} - \sin \beta} \quad \text{if } \theta_{23} > \theta_{12} \quad (6)$$

where β is the corner half angle and r_{ij} is radius of curvature of the fluid ij interface ($r_{ij} = \sigma_{ij}/P_{c,ij}$). The above constraints are based on purely geometrical arguments. These geometric conditions are necessary, but not sufficient for a stable layer formation [10]. Even if the geometrical criteria are satisfied, we compute the entry capillary pressures for the displacement without layer formation and compare it to the case with layer formation. The displacement that takes place is the one which requires less energy (i.e., lowest capillary entry pressure). The three-phase capillary entry pressure is computed following the extended MS-P method [10,11]. Thus, in our implementation intermediate layer formation and stability combines geometric and thermodynamic arguments.

Displacement Events

In the absence of viscous effects, bulk fluid displacements proceed through a series of equilibrium configurations with respect to capillary and buoyancy forces. The three-phase displacements considered here involve the injection of gas, oil or water into a network that contains initially at least two other phases. Although regions of the network may be occupied by one, two or all three fluids simultaneously, individual bulk displacements all involve the invasion of a pore element by a two-phase interface.

For a drainage dominated processes, where the non-wetting fluid is the invading phase, the following bulk displacements are accounted for:

- Direct drainage: fluid 1 → fluid 2 or fluid 3 recovered at the outlet
- Double drainage: fluid 1 → fluid 2 → fluid 3 recovered at the outlet
- Drainage-imbibition: fluid 1 → fluid 3 → fluid 2
fluid 2 → fluid 3 → fluid 1

Considering an imbibition dominated process, where either the intermediate wetting or the wetting fluid is injected, there are additional displacements taken into account:

- Direct imbibition: fluid 3 → fluid 1 or fluid 2 recovered at the outlet
fluid 2 → fluid 1 recovered at the outlet
- Double imbibition: fluid 3 → fluid 2 → fluid 1 recovered at the outlet
- Imbibition-drainage: fluid 3 → fluid 1 → fluid 2
fluid 2 → fluid 1 → fluid 3

Three types of displacement mechanisms are implemented: piston, snap-off, and cooperative pore body filling [4]. We do not consider multiple displacements beyond double displacements. The reason for this is that water is considered to be hydraulically connected everywhere in the pore network. Associated with each of these displacements is a threshold capillary pressure. Among all possible events, the one with the lowest (drainage dominated) or the highest (imbibition dominated) threshold capillary pressure is allowed. If necessary, this is accommodated by an increase/decrease of the invading phase pressure. We calculate the true three-phase capillary threshold pressures for the above displacements using the extended MS-P method [12].

Fluid Volumes and Conductances

If a pore or throat is occupied by one or only two of the fluids, the calculations of fluid volumes and hydraulic conductances are identical to that in two phase flow [13]. A comprehensive description of the mathematical details, including the effects of wettability, involved in these calculations has been presented earlier [13] and will not be repeated here. When three fluids are present, the total corner area open to flow is

$$A_c = r_{ij} \left[\cos \theta_{ij} (\cot \beta \cos(\theta_{ij} - \sin \theta_{ij}) + \theta_{ij} + \beta - \frac{\pi}{2}) \right] \quad (7)$$

r_{ij} is the radius of curvature and θ_{ij} is the corresponding contact angle. When gas is located in the centre of a pore, water resides in the corner (A_w) and there is an oil film in-between gas and water. The area occupied by oil thus $A_{oil} = A_c - A_w$. The conductance of the water layer in a corner is given by

$$g_w = C \frac{A_w^2 G_c}{\mu_w} \quad (8)$$

$$G_c = \frac{A_w}{4b_{ow}^2 \left[1 - \frac{\sin \beta}{\cos(\theta_{ow} + \beta)} (\theta_{ow} + \beta - \frac{\pi}{2}) \right]^2} \quad (9)$$

$$b_{ow} = r_{ow} \frac{\cos(\theta_{ow} + \beta)}{\sin \beta} \quad (10)$$

$$C = 0.364 + 0.28 \frac{G^*}{G_w} \quad (11)$$

$$G^* = \frac{\sin \beta \cos \beta}{4(1 + \sin \beta)^2} \quad (12)$$

where G_c is the shape factor for the corner section occupied by water, G^* is the shape factor without curvature on the interface, and b_{ow} is the distance from the apex of the corner to the location of the interface at the pore wall [see 4]. The correlation of parameters in this parameterization was tested using a 2D finite element code for incompressible laminar flow. For a variety of corner configurations, Equation (8) predicted the water conductance well within a 10 percent error margin for all possible combinations of the corner and contact angles. The conductance for the intermediate phase layer sandwiched between wetting and non-wetting phases is computed according to the formulation given by Patzek et al. [14].

Relative Permeabilities

To compute absolute and relative permeabilities, the flow of each phase in the network must be specified. For laminar flow, the flow rate of fluid i between two connecting pores I and J is given by

$$q_{i,IJ} = \frac{g_{i,IJ}}{l_{IJ}} (P_{i,I} - P_{i,J}) \quad (13)$$

where l_{IJ} is the spacing between the pore centres and $P_{i,I}$ is the pressure of fluid i in pore I and $P_{i,J}$ the pressure of fluid i in pore J . The effective conductance $g_{i,IJ}$ is assumed to be the harmonic mean of the conductances of the throat and the connected two half-pores. We invoke mass conservation at each pore

$$\sum_J q_{i,IJ} = 0 \quad (14)$$

where J runs over all throats connected to pore I . Equations (13) and (14) give rise to a set of linear equations for the pore pressures that are solved using standard numerical techniques. Constant inlet and outlet pressures are assigned as boundary conditions.

The absolute permeability k is computed initially when the network is fully saturated with water. From the computed pressure field, the total flow rate and thus the permeability are calculated using Darcy's law. Relative permeabilities are computed in the same fashion for the partially saturated network. The pressure in each phase is computed separately, assuming that all interfaces are fixed in place. The sum of flow rates through the inlet determines the macroscopic flow rate of that phase, which is inserted into the Darcy's law to compute its phase permeability k_i and $k_{ri} = k_i/k$.

MODEL VERIFICATION

To verify our model implementation, we computed three-phase drainage dominated relative permeabilities for reconstructed Berea sandstone and compared the results with experimental data reported by Oak [3]. The gas and oil relative permeabilities for gas

injection at S_{wi} are shown in Figures 1 and 2, respectively. Figure 3 shows the gas and water relative permeabilities for gas injection at S_{orw} . The value of the spreading coefficient used in the simulations is $S_{ow} = -2.0$ mN/m. The computed drainage dominated three-phase relative permeabilities for these two limiting two-phase cases are in fair quantitative agreement with the experimental data.

COMPARISON WITH STATFJORD EXPERIMENTS

Experimental Data

The experimental data on the Statfjord material comprise two-phase and three-phase steady-state relative permeability measurements reported by Petersen et al. [15]. All the flow measurements were performed in a vertical set-up. We reconstructed one of the plugs available from the composite core, based on thin section and SEM analysis. Fluid properties used in the flow simulations were the same as those for the experiments and are summarized in Table 1. Petrophysical properties and end point saturations for the reconstructed sample are compared with experimentally measured data in Table 2.

Two-Phase Relative Permeabilities

In this section, waterflood simulations are presented and compared with the two-phase experiments introduced by Petersen et al. [15]. First, primary drainage under strongly water-wet conditions was simulated to establish S_{wi} . Next, we simulated a waterflood to reach S_{orw} . In order to anchor the simulations to the experimental data, the wettability parameters in the model (i.e., contact angles) were varied. Figure 4 compares predicted and measured waterflood relative permeabilities. The results for the anchored waterflood simulations are in good quantitative agreement with the experimental data. The simulated Amott Index is found with $AI = 0.2$.

Three-Phase Relative Permeabilities

After a primary drainage simulation to reach S_{wi} we used the wettability parameters determined during the two-phase anchoring process as input parameters for the gas injection at S_{wi} . Following the nomenclatures used by Petersen et al. [15], this displacement series is denoted as **CDI**, indicating **C**onstant S_w , **D**ecreasing S_o , and **I**ncreasing S_g . The subsequent oil injection is termed **CID** series. The functionality of the three-phase model allows us next to simulate a gas injection after a (partial) waterflood (called **DDI** series) and the subsequent water injection (called **ICD** series), as reported in [15]. The value of the spreading coefficient used in all these simulations was $S_{ow} = -1.9$ mN/m.

CDI Series

The predicted relative permeabilities for the CDI process are compared with the experimental data in Figure 5. The computed results are again in fair quantitative agreement with the measured results. The computed S_{org} is very close to the experimental one (0.187 vs. 0.186). The predicted oil relative permeability is in good agreement with the experimental data across the entire saturation range. The computed gas relative permeability is in fair agreement with the measured data at low and high gas saturations, but tends to under-estimate the measured results at intermediate gas saturations. The cross-over point for the gas-oil relative permeabilities occurs at similar saturations, although the predicted values of the relative permeabilities are slightly lower than in the experiments.

CID Series

The predicted relative permeabilities for the CID process are compared with the measured results in Figure 6. The predicted relative permeabilities show fairly good agreement with the measured data in the high and intermediate gas saturation region. The computed $S_{gro} = 0.27$ is significantly larger than the measured $S_{gro} = 0.115$. We note that the measured S_{gro} is actually smaller than the $S_{org} = 0.186$ for the CDI process. This is surprising since gas is the non-wetting phase and the CID series thus represent an imbibition process.

The experiments reveal that a significant amount of gas has been displaced at the “bump” flow rate (from $S_g = 0.266$ to $S_g = 0.115$). The capillary number at the “bump” flow rate is of the order 10^{-4} . This is significantly larger than the critical capillary number required to remobilize trapped gas [16]. The large decrease in S_g at the “bump” flow rate might thus be caused by viscous forces remobilizing capillary trapped gas. This effect cannot be captured in the network model since the simulations assume that capillary forces dominate on the pore-scale.

Although the agreement between predicted and measured relative permeabilities for the CDI and CID series are encouraging, there exist a number of uncertainty sources that can contribute to the discrepancy between predicted and measured relative permeabilities. The measurements were done on a composite core, whilst the simulated results stem from one reconstructed plug. Consequently, there are uncertainties about how representative the reconstructed sample and its pore network representation are for the actual composite. Furthermore, the physical size of the composite core is orders of magnitude larger than the reconstructed model. This means that the buoyancy forces acting in the experiments (vertical set-up) are also orders of magnitude larger than in the simulations. We note that the measured gas relative permeability for the CID process (Figure 6) displays a clear non-monotonic behavior, whereas the measured gas relative permeability for the CDI series (Figure 5) shows a linear behavior at intermediate gas saturations. This suggests that buoyancy forces are important and affect the fluid distribution in the experiments and thus the measured relative permeabilities.

DDI Series

In the DDI displacement process, both oil and water are mobile and can be displaced. The starting point of the gas injection is obtained by performing a primary drainage to $S_w > S_{wi}$ directly followed by a waterflood terminating at $S_o > S_{orw}$. The saturation path obtained during the simulations (see Figure 7) shows that gas is first displacing connected oil and then displaces water and in turn part of the trapped oil (double displacement mechanisms). However, the experimental saturation path reveals that for each increase of gas saturation, both oil and water are displaced simultaneously and the produced amount is approximately constant (except for the first experimental data point).

In the simulations, capillary entry pressures determine the displacement sequence. The gas/oil displacement requires less energy than the gas/water displacement and therefore takes place first. The simulated saturation path is thus predicted solely by the displacement physics. A way to mimic the DDI steady-state experiments with simultaneous injection of multiple fluids would be to track the experimental saturation paths in the simulation and compute the corresponding relative permeabilities along

those paths. Although the functionalities of the network model allow multiple fluids to be simultaneously injected, we have not yet implemented a saturation path tracking algorithm to follow the measured saturation paths exactly.

CONCLUSION

A general three-phase network model that includes features, such as wettability alteration, intermediate phase spreading layers, and true three-phase capillary entry pressures, has been developed. The model allows injection of any immiscible fluid (gas, water, or oil) where the initial fluid distribution is established by a two-phase or a three-phase displacement process. This will allow us to closely reproduce common three-phase experimental displacement series (CDI, CID, DCI, ICD, DDI and IID). The model was applied to successfully compute three-phase relative permeabilities for CDI and DCI displacement series on water wet Berea samples reported by Oak [3].

The network model was next employed to simulate CDI and CID displacements for a non-water wet reservoir rock from the Statfjord field. In that context, we anchored the wettability parameters used in the simulations by reproducing experimentally measured two-phase relative permeabilities. Overall, the trends in the predicted three-phase relative permeabilities for the CDI/CID displacements are in fair agreement with the experimental steady-state results measured under in-situ conditions. Differences in relative values may be explained in terms of different sample size, pore-structure representativeness, and the balance between viscous, capillary, and buoyancy forces. Nevertheless, for a comprehensive validation of the model it is necessary to further investigate the differences observed between experiments and simulations.

The simulated results for the DDI displacement, with only a single phase injected, could not reproduce the measured saturation paths. Pore-scale simulations of three-phase steady-state experiments with injection of multiple fluids require the implementation of a saturation path tracking algorithm to ensure that the correct saturation paths are followed exactly. This will be investigated in future work.

ACKNOWLEDGEMENTS

StatoilHydro ASA is acknowledged for the development support and for granting permission to publish this work. Experimental data were acquired at IRIS.

REFERENCES

- [1] Piri, M.D., Blunt, M., "Three-Dimensional Mixed Wet Random Pore-Scale Network Modelling of Two- and Three-Phase Flow in Porous Media. II. Results", *Physical Review E*, 2005, **71**, 026302-1-11.
- [2] van Dijke, M.I.J., M., Sorbie, K.S., Sohrabi, M., Tehrani, D., and Danesh, A., "Three-phase flow in WAG processes in Mixed-wet porous media : pore-scale network simulations and comparison with micromodel experiments" *SPEJ* 9(1), 57-66.
- [3] Oak, M.J., "Three-phase relative permeability of water wet Berea", SPE/DOE 20813, *Proceedings of the SPE/DOE Symposium on EOR*, Tulsa, OK, April 1990.
- [4] Øren P.E., Bakke, S., and Arntzen, O.J., "Extending Predictive Capabilities to Network Models", *SPEJ*, December 1998, 324-336.

- [5] Øren, P.E. and Pinczewski, W.V., "Effects of Wettability and Spreading on Recovery of Waterflood Residual Oil by Immiscible Gas Flooding", *SPE Formation Evaluation*, 1994, **9**, 149-156.
- [6] Øren, P.E. and Pinczewski, W.V., "Fluid Displacements and Pore-Scale Displacements in Drainage Dominated Three-Phase Flow", *Transport in Porous Media*, 1995, **20**, 105-133.
- [7] Blunt, M., Zhou, D., Fenwick, D., "Three-Phase Flow and Gravity Drainage in Porous Media", *Transport in Porous Media*, 1995, **20**, 77-103.
- [8] Bartell, F.E and Osterhoff, H.J., *Ind. Eng. Chem.*, 1927, **19**, 1277-1280
- [9] van Dijke M.I.J.; Sorbie K.S.; McDougall S.R., "Saturation-dependencies of three-phase relative permeabilities in mixed-wet and fractionally wet systems" *Advances in Water Resources*, Volume 24, Number 3, February 2001 , pp. 365-384(20).
- [10] Van Dijke, M.I.J., and Sorbie, K.S., "Existence of Fluid Layers in the Corners of a Capillary with Non-Uniform Wettability", *J. Coll. & Interf. Sci.*, 2006, **293**, 455-463.
- [11] Piri, M.D., Blunt, M., "Three-Phase Threshold Capillary Pressures in Noncircular Capillary Tubes with Different Wettabilities Including Contact Angle Hysteresis", *Physical Review E*, 2004, **70**, 061603-1-17.
- [12] van Dijke M.I.J., Piri, M., Blunt, M.J., and Sorbie K.S. "Criterion for three-fluid configurations including layers in a pore with non-uniform wettability", *Proceedings of CMWR-XVI Symposium*, 2006 Copenhagen, Denmark.
- [13] Øren, P.E., Bakke, S., "Reconstruction of Berea Sandstones and Pore-Scale Modeling of Wettability Effects", *J. Pet. Sci. & Eng.*, 2003, **39**, 177-199.
- [14] Al-Futaisi A., and Patzek T.W., "Three-Phase Hydraulic Conductance in Angular Capillaries" *SPE 75193 presented at the 2002 SPE/DOE Symposium on Improved Oil Recovery* held in Tulsa, OK , April 2002.
- [15] Petersen, E.B.Jr., Lohne, A., Vatne K.O., Helland, J.O., Virnovsky, G., Øren, P.E., "Relative permeabilities for two- and three-phase flow processes relevant to the depressurization of the Statfjord field *International Symposium of the Society of Core Analysts*, Abu Dhabi, UAE, 2008.
- [16] Ding, M., Kantzas, A. "Investigation of critical capillary number for gas-water system through experiment and reservoir simulation" *International Symposium of the Society of Core Analysts*, Abu Dhabi, UAE, 2008.

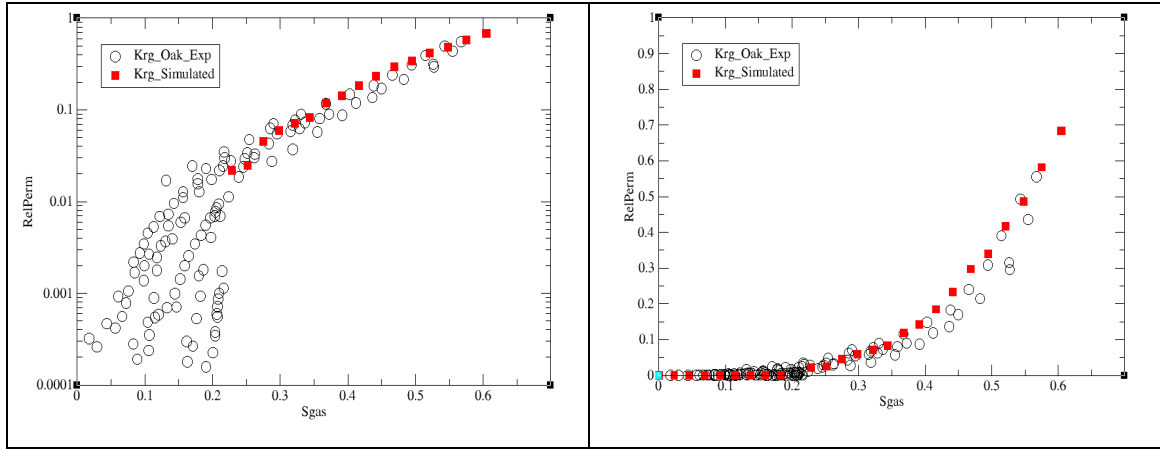


Figure 1: Comparison of computed gas relative permeability (red squares) against experimental measurements (black circles) for a Berea sandstone.

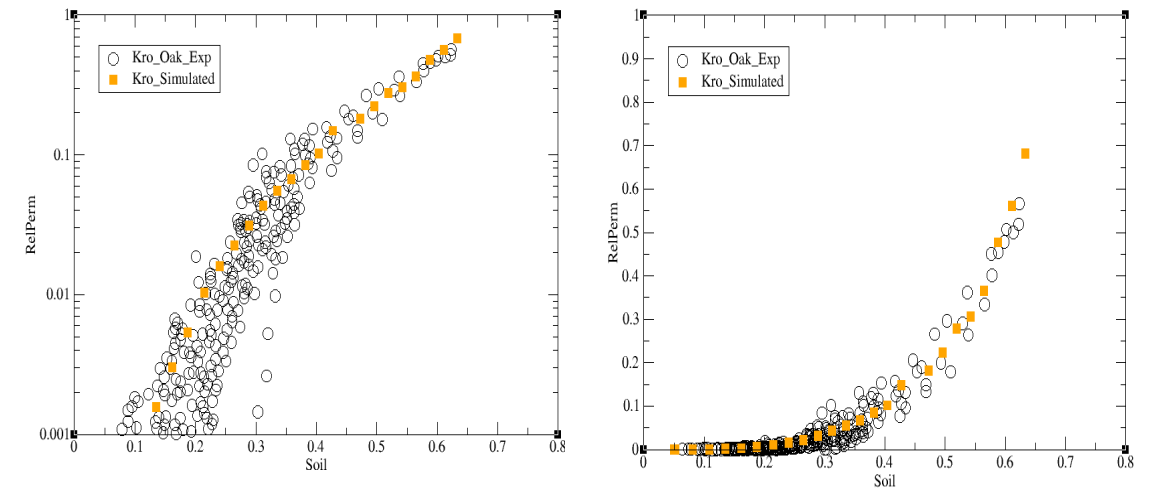


Figure 2: Comparison of computed oil relative permeability (orange squares) against experimental measurements (black circles) for a Berea sandstone.

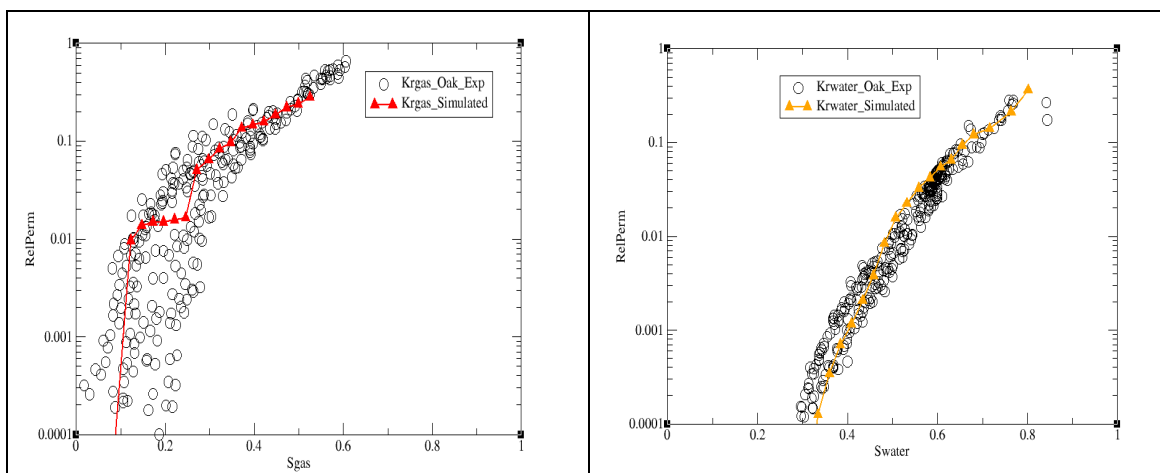


Figure 3: Comparison of computed gas (left) and water (right) relative permeabilities against experimental measurements for a Berea sandstone.

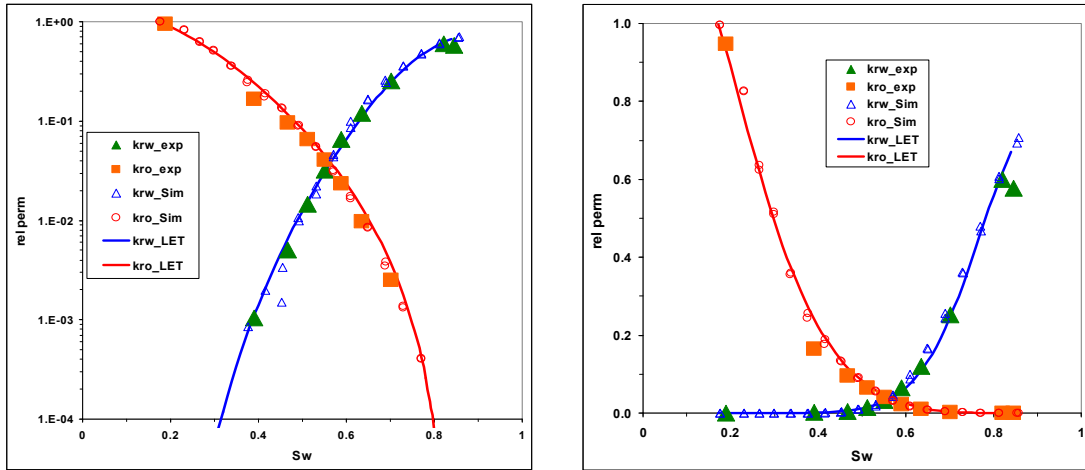


Figure 4: Two-phase waterflooding experimental vs. simulated oil and water relative permeabilities.

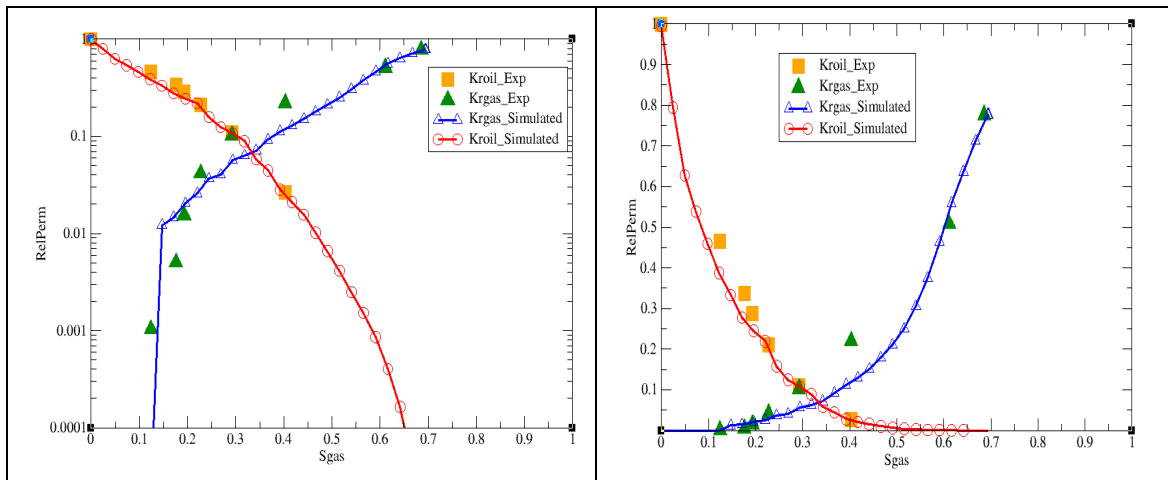


Figure 5: CDI series relative permeabilities (gas and oil) logarithmic (left chart) and linear (right chart).

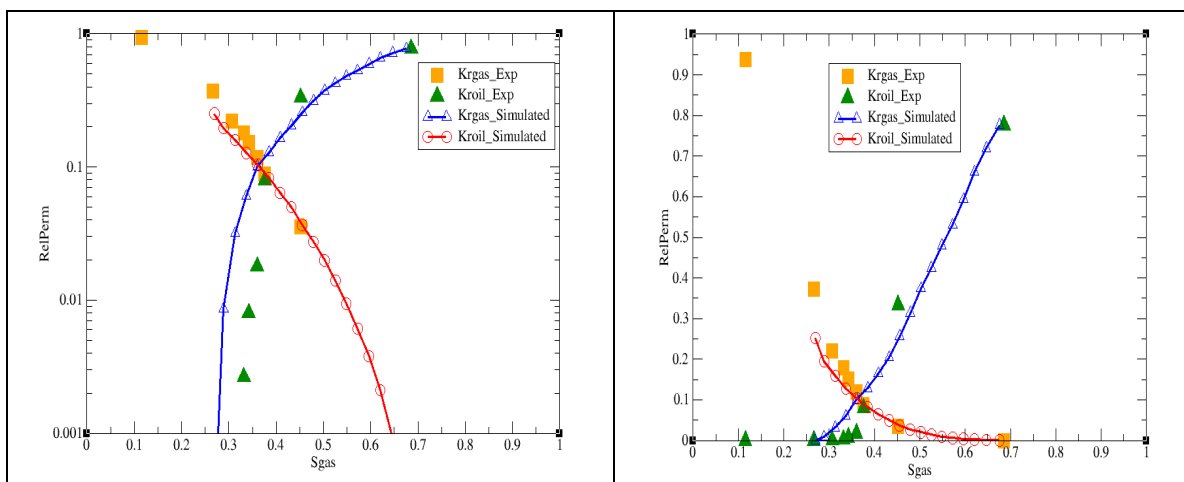


Figure 6: CID series relative permeabilities (gas and oil) logarithmic (left chart) and linear (right chart).

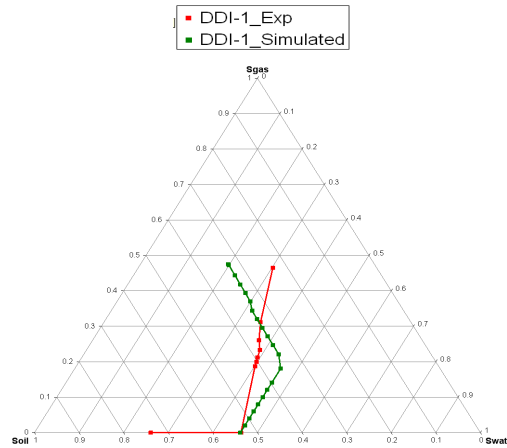


Figure 7: Saturation path for DDI-1 series.

Table 1: Fluid data from Petersen et al. [15]

	Water	Oil	Gas
Density (g/cc)	1.0013	0.6911	0.1642
Viscosity (cP)	0.336	0.423	0.0218
Interfacial tension* (mN/m)	Oil/water	gas/oil	gas/water
	23.1	3.8	22.5

* Pendent drop method at test conditions (91°C and 200 bars).

Table 2: Petrophysical parameters measured and computed for the composite core material

	Measured	Computed
Absolute Permeability (mD)	1282	1872
Total Porosity (fraction)	0.351	0.334
S_{wi} (fraction)	0.19	0.20
S_{orw} (fraction)	0.15	0.12
k_{rw} (end point)	0.58	0.57